Magn Reson Mater Phy (2014) 27:149–159
DOI 10.1007/s10334-013-0388-1

REVIEW ARTICLE

Characterization of the impact to PET quantification and image quality of an anterior array surface coil for PET/MR imaging

Scott D. Wollenweber · Gaspar Delso · Timothy Deller · David Goldhaber · Martin Hüllner · Patrick Veit-Haibach

Received: 12 February 2013 / Revised: 13 May 2013 / Accepted: 3 June 2013 / Published online: 26 June 2013

Abstract
Object The aim of this study was to determine the impact to PET quantification, image quality and possible diagnostic impact of an anterior surface array used in a combined PET/MR imaging system.
Materials and methods An extended oval phantom and 15 whole-body FDG PET/CT subjects were re-imaged for one bed position following placement of an anterior array coil at a clinically realistic position. The CT scan, used for PET attenuation correction, did not include the coil. Comparison, including liver SUV_{mean}, was performed between the coil present and absent images using two methods of PET reconstruction. Due to the time delay between PET scans, a model was used to account for average physiologic time change of SUV.
Results On phantom data, neglecting the coil caused a mean bias of −8.2 % for non-TOF/PSF reconstruction, and −7.3 % with TOF/PSF. On clinical data, the liver SUV neglecting the coil presence fell by −6.1 % (±6.5 %) for non-TOF/PSF reconstruction; respectively −5.2 % (±5.3 %) with TOF/PSF. All FDG-avid features seen with TOF/PSF were also seen with non-TOF/PSF reconstruction.
Conclusion Neglecting coil attenuation for this anterior array coil results in a small but significant reduction in liver SUV_{mean} but was not found to change the clinical interpretation of the PET images.

S. D. Wollenweber · G. Delso (✉) · T. Deller · D. Goldhaber
GE Healthcare, Waukesha, WI, USA
e-mail: gaspar.delso@ge.com

S. D. Wollenweber
e-mail: Scott.Wollenweber@med.ge.com

G. Delso · M. Hüllner · P. Veit-Haibach
University Hospital, Zurich, Switzerland

Keywords Positron-emission tomography · Magnetic resonance imaging · Attenuation correction

Introduction

In a dedicated PET/MR imaging system, traditional methods of accounting for PET attenuation cannot be utilized. Several publications [1–3] have explored the use of segmentation of MR image data to obtain the patient component of attenuation, but several challenges remain [4–6]. One significant challenge is in the area of MR surface coils. Depending on the coil design, significant artifacts and quantification errors can occur in the PET images if the coil is not accounted for in the attenuation map used in image reconstruction [7–11]. The impact of the coil depends on the placement of the coil relative to the patient, as well as the location within the coil of any dense, compact elements.

To characterize an impact, several important PET metrics imaging should be considered. The first goal of a PET study is to detect normal and abnormal radiotracer uptake throughout the body. Image artifacts can occlude important diagnostic findings, such as when streak artifacts projecting back through the image hinder location of a high-uptake lesion or evaluation of normal anatomy. The second goal in PET is to localize an area of interest, typically an FDG-avid tumor in whole-body oncologic PET. For this purpose, the spatial accuracy and spatial invariance of quantification accuracy are important. To localize a feature and understand its relationship to nearby structures, visual inspection of the images, including use of both PET and CT or MR images, is typically performed. In some cases, margins may be defined through use of automated segmentation or manual delineation to define the extent of the tumor. A third goal of quantitative PET is to determine the actual

radiotracer uptake of the area-of-interest. This goal often has multiple elements, including definition of a volume-of-interest (VOI) in a reference organ (e.g. liver), as well as the standard uptake value (SUV) of a lesion. Given that there are multiple diagnostic requirements of the image data, multiple metrics should be used to determine how well the above goals are met. Therefore, multiple measures were considered in this study and used to determine the impact of an MR anterior array (AA) surface coil within a PET/MR imaging system.

In performing this study, PET image data at multiple time points must be compared—in this case, data from a bed position acquired during a whole-body series of bed positions without the AA coil to that from a bed position acquired later with the coil positioned on the patient. Since PET data is typically decay-corrected to the start of the scan, the single bed position with the AA coil present required further decay correction to the start of the whole-body study. A more difficult and potentially confounding parameter, however, was accounting for any bio-redistribution that occurs during the time between scans. Uptake timing is often considered when the standardization of imaging protocol is of importance [12–14], but it is also realized that dual time-point PET has potential diagnostic use because of the bio-redistribution [15, 16], although there is some discrepancy concerning its clinical relevance. Since the effects due to the presence of the coil are hypothesized to be small, <10 % change in SUV, the effect of bio-redistribution was included as a contributor to differences between scans since tissue volume SUVs were compared at multiple time points. However, all of these effects might be just of technical or hypothetical nature and therefore the actual diagnostic impact on a clinical routine readout of those studies must also be considered.

The aim of this study was to determine the impact of an anterior array surface coil if an attenuation map for the coil is neglected within PET image reconstruction in a dedicated PET/MR imaging system. The impact was measured by considering PET images and image difference maps (with/without AA coil), SUV quantification in the liver and per-pixel SUV joint histogram analysis. The impact with use of time-of-flight (TOF) PET as compared to non-TOF PET was also evaluated under the hypothesis that use of the TOF information helps localize the impact of the attenuation data inconsistency when neglecting the coil attenuation [17]. Lastly, a clinical routine read-out of the scans with and without the coil was performed and the readers determined the clinical impact.

Materials and methods

Phantom study

A phantom study was conducted using the AA coil on the top of an extended oval phantom (25.3 L) using the arrangement shown in Fig. 1a. The phantom (Data Spectrum™, Hillsborough NC) was filled with a uniform distribution of ^{18}F-FDG. Using a Discovery 690 PET/CT system (GE Healthcare, Waukesha WI) PET scans were subsequently acquired without and with the AA coil. A CT scan was acquired with no coil present, for the purpose of attenuation correction for both coil-present and coil-absent scans. The total activity was 159.0 MBq (6.3 kBq/mL) at the beginning of the scan without coil, and 105.5 MBq (4.2 kBq/mL) at the beginning of the scan with coil. The acquisition times were set such that both scans acquired an equivalent number of annihilations (60 and 102 min, respectively).

PET image reconstruction of the phantom, with both non-TOF and TOF, used a 192 × 192 grid over 400 mm transaxial FOV and two iterations, and 24 subsets of OS-EM followed by a 4.0 mm Gaussian post-filter. Images were compared at three axial locations and a PET SUV image joint histogram analysis was performed for voxels in the range of 0.1–2.5 SUV (g/ml). The SUV value of the

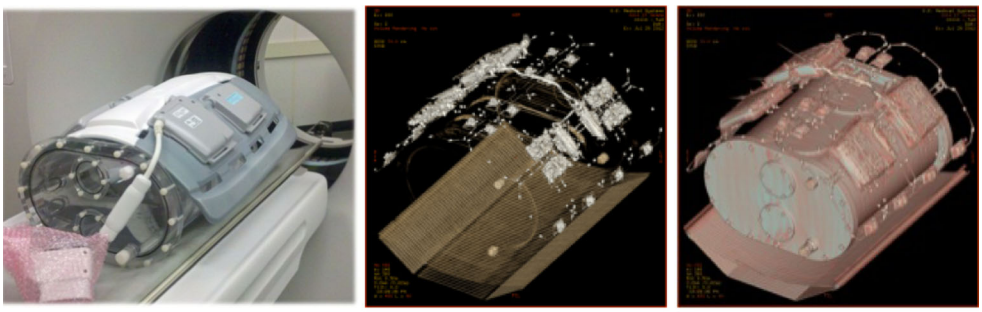

(a) (b) (c)

Fig. 1 The GE GEM anterior array coil measures 55.6x67.4x3.3 cm, weighs 2.8 kg and is mainly made of foam, with Lexan plastic for feed and decoupling board housing. The cable is connected to the upper right board, weights 1.1 kg and has a diameter of 11 mm, including insulation. **a** Photograph of the anterior array coil placed onto a uniformly filled oval phantom. **b** Render of an oblique view CT image of the coil placed onto an extended oval phantom. **c** Same view at a different render level

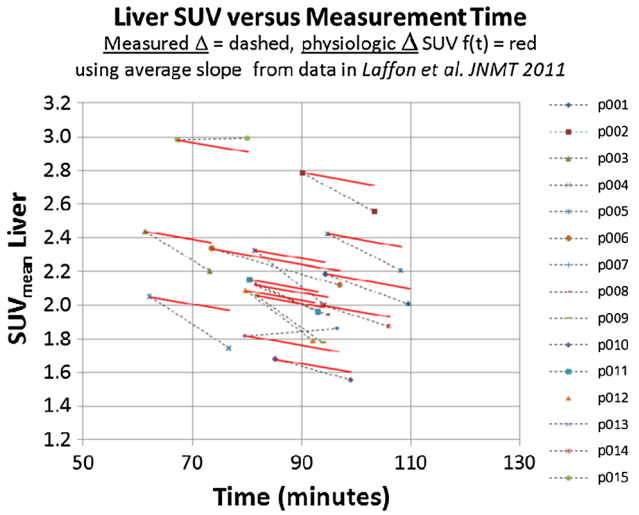

Fig. 2 Plot for all 15 patients of liver SUV_{mean} showing the early time point (coil-absent) and later time point (coil-present). The *red lines* indicate expected normal liver FDG SUV change over the same time period

difference (coil present, coil absent) images was also calculated and the average SUV values from two representative regions in the difference images were found.

Clinical data acquisition

Fifteen patient studies were acquired with whole-body FDG PET/CT imaging. The imaging protocol included 14–18 min for whole-body PET/CT acquired depending on the size of the patient. The average patient weight was 72 ± 12 kg, the average BMI was 26 ± 5 kg/m^2 and the average FDG dose was 310 ± 13 MBq. The present study did not involve any extra radiation dose delivered to the patients. First, a helical CT scan covering the PET imaging field-of-view (FOV) was acquired and subsequently used for attenuation correction of all PET data, including when the AA coil was present. Next, 6–8 bed positions were acquired for whole-body FDG PET imaging. After the whole-body scan completed, the patient was transported out of the imaging bore and the AA coil was placed by the technologists at a 'typical use' location. Thus, each patient had a somewhat different location of the AA coil. Notice that, given the coil dimensions, the liver was covered in all cases. Finally, out of all the bed positions defined and acquired during the routine PET/CT scan, the one currently covered by the coil was re-acquired such that the patient was at the same nominal location as during the whole-body scan. This bed position always had partial coverage of the liver, enabling the impact on liver tissue uptake to be measured and compared. The average time between the bed position imaged with AA coil and the 'no-coil' bed position (within the whole-body scan) was 14.0 ± 2.9 min. PET image comparisons were performed in SUV units, hence the decay time between scans was not a factor in the analysis.

PET images were formed using a fully-3D OS-EM iterative reconstruction (VuePoint HD) with two iterations, and 24 subsets onto a 256 × 256 image grid (2.73 × 2.73 × 3.27 mm voxels) over a 700 mm diameter FOV. Images were filtered in image space using a 4.0 mm FWHM in-plane Gaussian filter followed by an axial filter with a 3-slice kernel using relative weights of 1:4:1. All quantitative corrections, including normalization, dead-time, randoms, scatter and attenuation, were applied during image reconstruction. The TOF image reconstructions (VuePoint-FXS) used the same reconstruction parameters except with three iterations and 18 subsets and included point-spread-function (PSF) compensation. It is worth pointing out that the single-bed reconstructions with the AA coil placed on top of the patient's body are expected to have increased but unbiased noise near the axial end slices.

This investigation was performed in collaboration between GE Healthcare and the Department of Medical Imaging, University Hospital, Zurich, Switzerland.

Clinical data analysis

For each patient, the location of a liver VOI of size 7 × 7 × 7 voxels, or approximately 8.4 ml, was determined from the reconstructed PET images. Voxels within the VOI were averaged to find the SUV_{mean} in g/ml in order to compare the data with the AA coil present to that from the standard clinical data without the coil. A percent difference between the liver SUV_{mean} with and without the coil was plotted along with the mean and ±1 standard deviation across studies. Paired *t* tests were performed to determine significance of with- versus without-coil results.

In order to compare liver SUV at two time points, the physiologic change in FDG distribution in liver was taken into account using the data from Laffon et al. [18]. Their work presented data from 11 patients where two measurements of SUV_{mean} in a liver VOI were found at two times post-FDG injection. For each of these 11 patients, the rate-of-change slope (ΔSUV/Δtime) was calculated [first time point 72.2 ± 11.6 min (55.0, 89.0), second time point at 158.6 ± 19.6 min (130.0, 194.0), average time between points 86.5 ± 16.6 min (63.0, 115.0)]. Assuming that change between the time points was linear and that the data were representative of the same population used in our study, the amount of expected SUV change could be accounted for between the coil-absent data and the coil-present data in order to account for expected normal bio-redistribution change.

Besides the localized error measures provided by VOI analysis, joint image histograms of voxel-wise PET SUV were generated, in order to compare the overall results with

and without the coil. Voxels from both images that were between 0.1 and 5.0 g/ml were included in the plots. A regression line was determined from the data with intercept forced through the origin. The slope of the line and the adjusted R^2 were found for each patient comparison with and without the AA coil.

All comparisons were done between coil-present and coil-absent images using the TOF images as well as using the non-TOF images.

Diagnostic evaluation

To determine the influence of the coil on the PET data, several parameters were assessed qualitatively in the same manner as was used in typical clinical routine. One dual board-certified radiologist/nuclear medicine physician and a board-certified radiologist with substantial nuclear medicine experience evaluated the images. The following four sets of images were evaluated: (a) TOF without coil (reference study), (b) TOF with coil, (c) non-TOF without coil, and (d) non-TOF with coil. It was determined by the clinical readers (1) whether any lesion was detected within the FOV, (2) whether lesions were perceived as qualitatively equal in all studies, using as a reference the TOF PET-CT without coil, (3) whether the clinical report would have been changed based on the coil-present images and (4) whether reader confidence changed concerning the characterization of any lesion. Qualitative parameters for evaluation (2) included rating the sharpness of lesions using a 4-point scale: 1 = sharp, 2 = blurring noted on some edge pixels, 3 = blurring noted on most edge pixels, 4 = entire lesion blurred. The conspicuity of a lesion's border, as well as its localization with respect to the reference study, were also determined.

Results

Phantom study

A set of images with and without the AA coil on the extended oval phantom using non-TOF PET reconstruction (VuePoint HD) and TOF reconstruction (VuePoint FX) are shown in Fig. 3. The joint histogram results comparing the PET phantom images with and without the AA coil are shown in Fig. 4. The results of VOI analysis are shown in Fig. 5. Two representative areas were measured and found to have biases of −2.3 and −14.2 % for non-TOF/PSF reconstruction. With TOF/PSF, the biases were, respectively, −5.4 and −9.2 %. The mean reconstructed SUV was measured to be 1.13 g/mL without TOF and 1.07 g/mL with TOF. These deviations from the ideal 1.00 g/mL are within the expected range for this kind of measurement, and can be explained by the accuracy of the dose calibrator measurement, the phantom volume measurement and the system corrections (e.g. the scatter model).

Clinical study

The average time from injection to scan start was 80.6 min [±10.7 min, range (61.5, 94.8)]. The average delay time between coil-absent and coil present scans was 14.0 min [± 2.9 min, range (11.9, 23.4)]. From the data in [18], the slope for rate of change in liver SUV_{mean} was $-5.5 \pm 1.3 \times 10^{-3}$ (g/ml/min) and was very consistent over the 11 patients included in that study. This rate of change was applied to each of the 15 studies based upon its time difference between coil-absent and coil-present scanning and subtracted from the observed difference. Over the 15 studies, this accounted for, on average, a 3.5 % portion of the difference observed in liver SUV_{mean}.

A plot of the decay-corrected liver SUVs for the 15 patients comparing coil-absent with coil-present images is shown in Fig. 2. These data represent the PET image measurements using TOF reconstruction. Note how, in three cases, data were acquired before the liver activity peak estimated by Laffon et al. This could, potentially, cause a minor masking of the impact of hardware attenuation on the second measurement.

A chart showing the comparison between coil-absent and coil-present liver VOI SUV_{mean} for both TOF and non-TOF data is shown in Fig. 6. The numeric results are contained in Table 1. The plot in Fig. 7 shows the percent differences between coil-absent and coil-present liver VOI SUV_{mean} for both TOF and non-TOF image reconstructions.

PET axial, sagittal and coronal images, without and with the AA coil, from a representative patient are shown in Fig. 8. These images utilize the TOF and PSF within image reconstruction. Figure 9 shows the non-TOF, no PSF axial images without and with AA coil for this same patient. Results from the other patients were similar to those shown in this example.

Joint histograms for these two patient studies are shown in Fig. 10 using a logarithmic color scale for frequency. Notice that these histograms do not account for the biodistribution of the radiotracer in the liver over time. Joint histograms for other datasets were similar except for P015, which had a joint histogram fit slope of 0.995 for both non-TOF and with TOF/PSF comparisons. The joint histogram fit results for all patients and both reconstruction methods are shown in Table 2.

Change in liver SUV comparing presence and absence of the AA coil was evaluated using a paired *t*-test for the PET images with TOF and PSF: the mean difference between coil-present and coil-absent was significant ($M = 0.112$ g/ml, $SD = 0.110$, $N = 15$), with $t(15) = 3.94$, two-tail

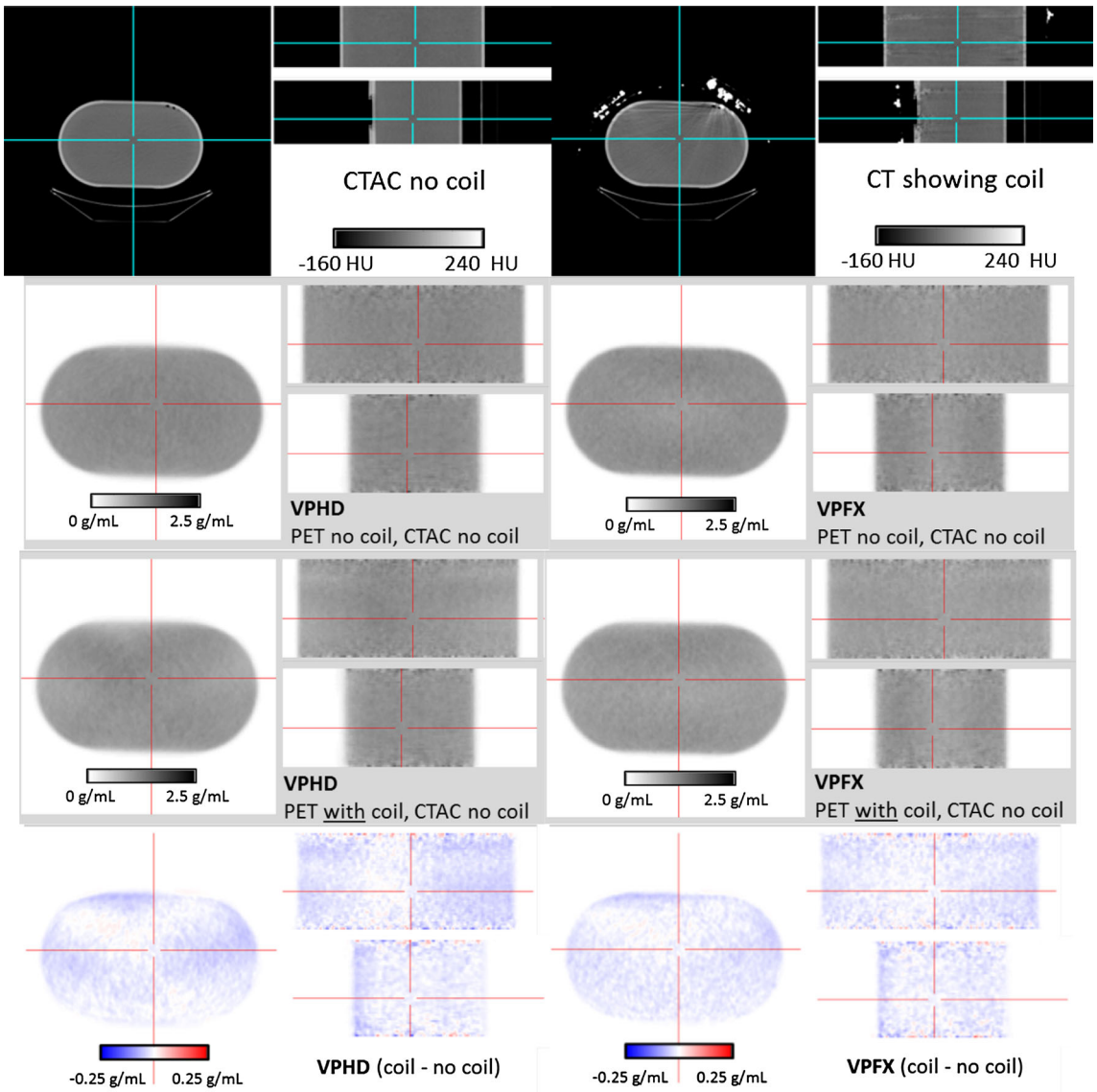

Fig. 3 PET/CT images without and with the AA coil present, for a central axial slice location, using non-TOF (*left*) and TOF PET reconstruction. In all cases, the attenuation correction did not include the coil. PET coil/no coil difference images are shown in the *bottom row*

$p = 0.001$ and a 95 % C.I. about the mean difference of [0.05, 0.17]. With the non-TOF/PSF PET images, the mean difference was also significant (M = 0.142 g/ml, SD = 0.137, $N = 15$), with t(15) = 4.01, two-tail $p = 0.001$ and a 95 % C.I. about the mean difference of [0.07, 0.22]. Both PET image reconstruction methods showed a significant, measureable difference in liver SUV in the VOI, albeit this was only a 5 % difference on average across the patients. The range of the liver SUV differences between images with and without the AA coil using TOF/PSF was [−11.5, 7.8 %] and using non-TOF/PSF PET images was [−5.6, 11.2 %], after accounting for the average FDG liver uptake change over time.

To understand the utility of the PET TOF information, the significance of the slope of the joint histogram linear fit comparing presence and absence of the AA coil was evaluated using a paired t test for the two PET image reconstruction methods. The mean of the slope difference was significant (M = 0.012, SD = 0.006, $N = 15$), with $t(15) = 7.58$, two-tail $p = 2.54\text{e-}06$, and a 95 % C.I. about the mean slope difference of [0.008, 0.015]. These results provide evidence that using the TOF information produced a more accurate overall PET SUV image in the presence of the un-accounted coil attenuation.

The clinical diagnostic evaluation revealed 13 pathological lesions in seven of the 15 patients. All lesions were detected in all four types of PET images (with and without coil, with and without TOF/PSF). However, slight qualitative differences were noted. In three patients, the lesion and the normal anatomical structures were noted to

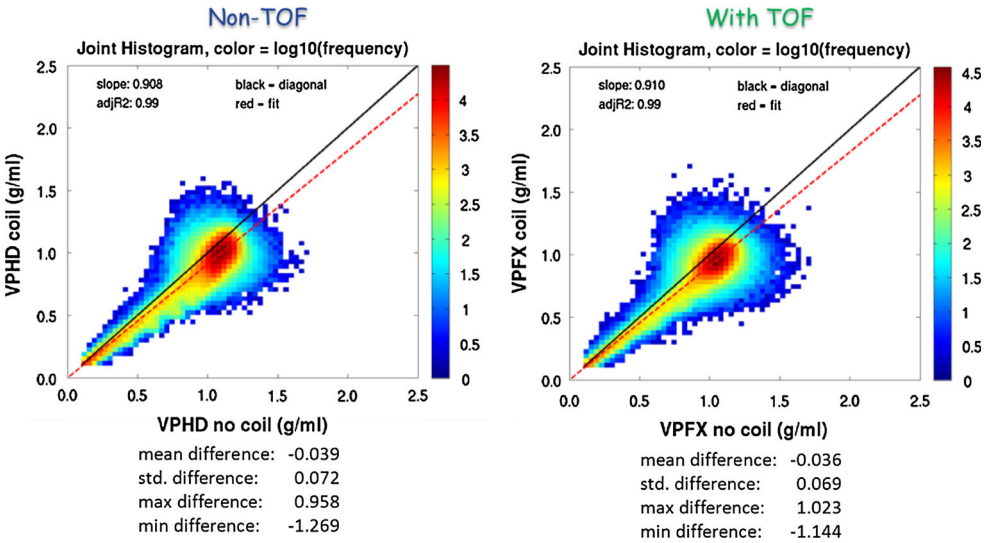

Fig. 4 Joint histogram of PET images comparing with AA coil to without AA coil for non-TOF (*left*) and with TOF (*right*). PET image voxels between 0.1 and 2.5 g/ml were included in the analysis. A linear fit through the origin is shown. Statistical results of the difference images for the two reconstruction methods are shown below the histograms

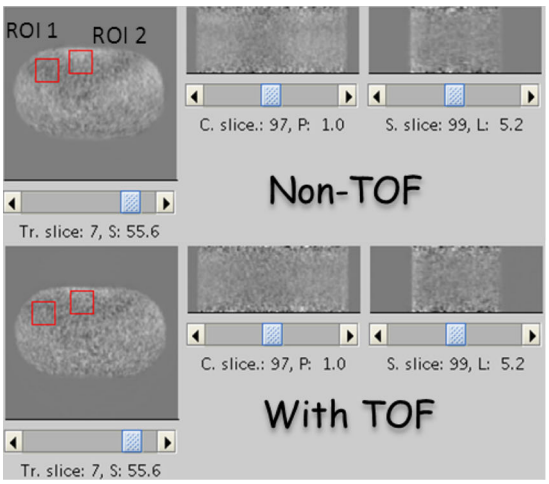

SUV	*non-TOF*		*with TOF*	
(C-nC)	ROI 1	ROI 2	ROI 1	ROI 2
mean	-0.026	-0.160	-0.058	-0.098
Avg % diff.:	8.2%		7.3%	
std.	0.062	0.101	0.066	0.090
min	-0.176	-0.399	-0.229	-0.295
max	0.134	0.082	0.150	0.121
BGD g/ml:	1.13		1.07	

Fig. 5 PET axial, coronal and sagittal difference images of the oval phantom (with—without coil) for non-TOF and TOF PET images. ROI analysis results are also shown for the two regions marked as red boxes in the images. The mean SUV was 1.13 g/mL for non-TOF reconstruction and 1.07 g/mL with TOF

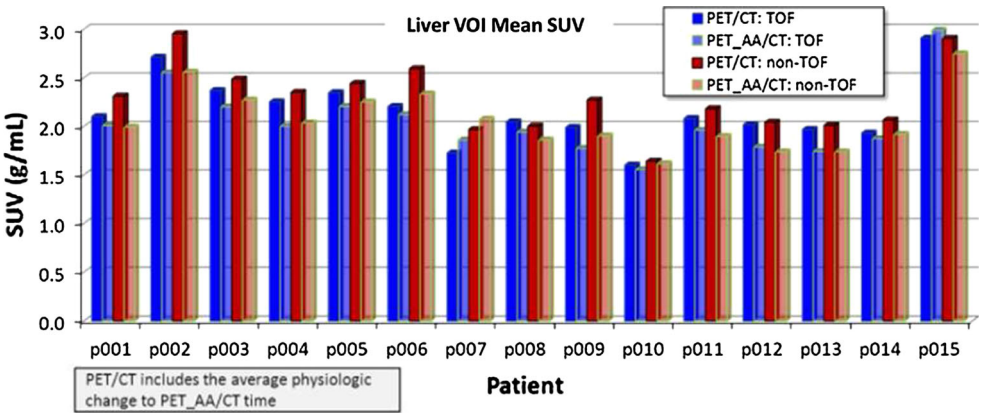

Fig. 6 *Bar chart* of all liver VOI SUV_{mean} values comparing coil-absent (PET) to coil-present (PET_AA) for both TOF and non-TOF reconstructions

be less sharp (ranked 3 on the aforementioned four-point scale) in the coil-present image. In all other patients and lesions, no qualitative difference was noted. The opposite occurred in one patient, where a slight overlap artifact within the liver between the bed positions was absent on the coil-present (single-bed-position) images. Overall, and most importantly, the readers would not have changed their report concerning the diagnostic results or concerning the characterization of the lesions. Furthermore, no difference in reader confidence was noted between the TOF-with-coil images and TOF-without-coil images. However, as expected, all non-TOF (non-PSF) images

Table 1 Results for liver SUV_{mean} for the 15 subjects, including the coil present/absent comparison within PET reconstruction methods

Liver SUV_{mean}/ $N = 15$	PET/CT: non-TOF (-physio)	PETAA/CT: non-TOF	PET/CT: TOF/PSF (-physio)	PETAA/CT: TOF/PSF
Avg	2.20	2.06	2.15	2.04
Std	0.36	0.32	0.34	0.36
Max	2.88	2.75	2.91	2.99
Min	1.56	1.62	1.60	1.55
Avg. % diff., account for physio Δ	Avg	−6.1° %		−5.2 %
	Std	6.5° %		5.3 %
	Max	10.7° %		7.8 %
	Min	−13.7 %		−11.5 %

Physiologic SUV change (3.5 % on average) has been individually accounted for

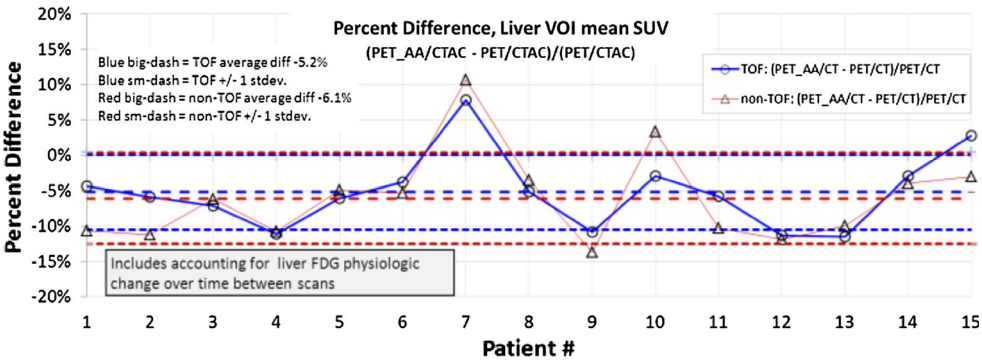

Fig. 7 Plot of the coil-absent/coil-present percent differences per patient of the liver VOI SUV_{mean} for each image reconstruction method (TOF, non-TOF)

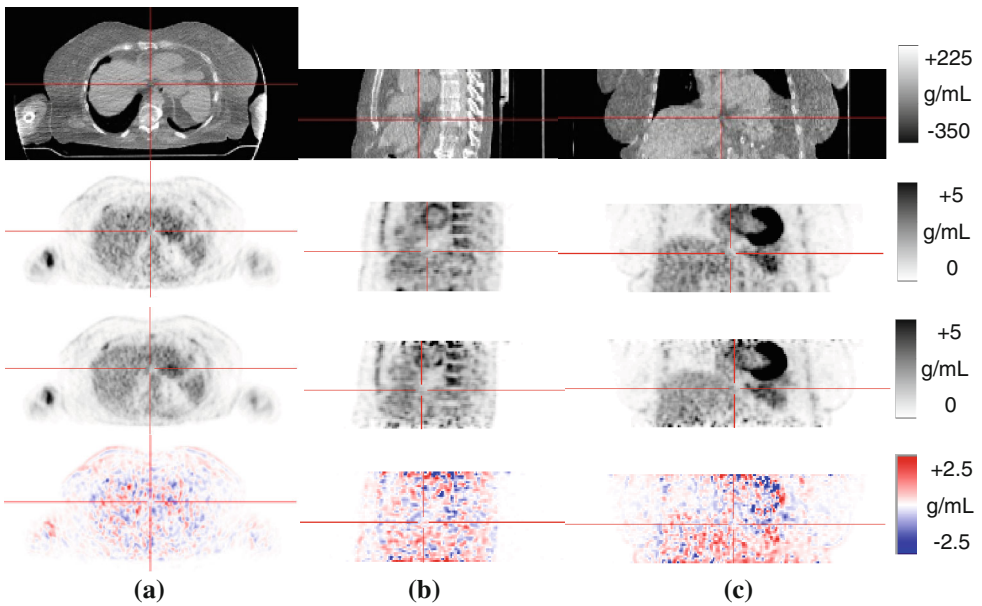

Fig. 8 Patient P011 axial (**a**), sagittal (**b**) and coronal (**c**) images of, from *top* to *bottom*: CT scan; TOF PET without AA coil; TOF PET with coil; and PET SUV absolute difference images (PET/CT—PET_AA/CT). SUV images are shown with window [0, 5] g/ml and difference images are with a [−2.5, 2.5] g/ml window

were rated as more blurry/less sharp than the TOF/PSF images with a typical lesion rank of 3.

Discussion

Given the design of the AA coil used in this study, the initial hypothesis was that the net effect would be less than 10 % on the quantitation for PET. In contrast, Martinez-Möller et al. [1] reported average SUV changes up to 13 %, using their 4-class MR-based attenuation correction approach, whereas Keereman et al. [3] claim errors up to 5 % using a 5-class approach.

The results demonstrate that the coil, while having a measureable impact on PET quantitation, has little impact on clinical image quality for both PET reconstruction approaches. This is confirmed by the results of the phantom study, which show that the bias introduced by the coil

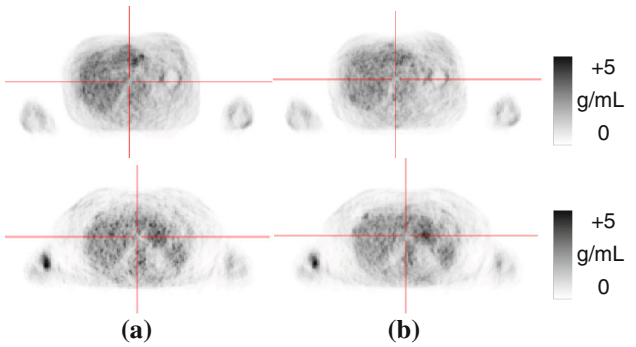

Fig. 9 Non-TOF/PSF axial PET images for two patient cases: P004 (*top row*) and P011 without **a** and with **b** AA coil

presence (as high as −14.1 % when no TOF information is used) has a low-frequency pattern that is less susceptible to lead to clinically relevant errors.

In order to measure a small impact in quantitation for a dual-time-point FDG-PET study, a first order approximation of the model in [18] was used, assuming the behavior they observed applied to the subjects included in this study (note how Laffon's measurements are approximately 90 min apart, in contrast to approximately 15 min in the present study). While this is not proven as part of this study, it was considered reasonable to include such a term describing the FDG wash-out as well as to use the model

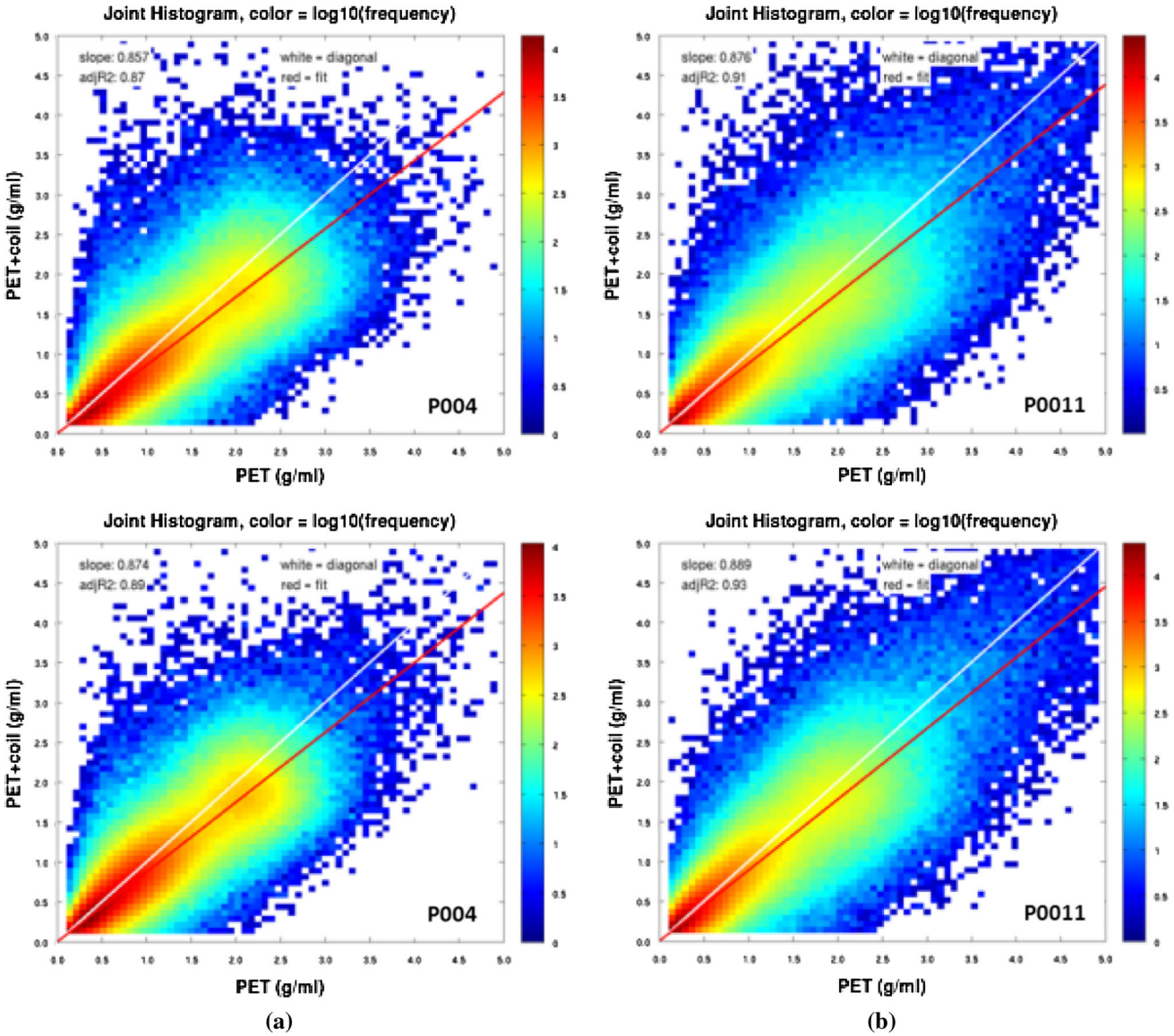

Fig. 10 Joint histograms with a logarithmic frequency scale for P004 **a** and P011 **b** with non-TOF/PSF (*top row*) and with TOF/PSF (*bottom row*). Note how these do not account for the effect of tracer redistribution

Table 2 Linear fit slope and adjusted R^2 for voxels with joint SUV between [0.1, 5.0], all patients and both reconstruction methods

	Non-TOF/PSF		TOF/PSF		Slope (TOF-nonTOF)
	Slope	R2	Slope	R2	
p001	0.888	0.680	0.906	0.640	0.018
p002	0.854	0.830	0.870	0.850	0.016
p003	0.905	0.860	0.918	0.870	0.013
p004	0.857	0.870	0.874	0.890	0.017
p005	0.853	0.870	0.861	0.870	0.008
p006	0.838	0.800	0.855	0.830	0.017
p007	0.891	0.880	0.893	0.900	0.002
p008	0.885	0.820	0.902	0.850	0.017
p009	0.855	0.840	0.866	0.870	0.011
p010	0.898	0.870	0.906	0.890	0.008
p011	0.876	0.910	0.889	0.930	0.013
p012	0.859	0.880	0.871	0.890	0.012
p013	0.870	0.870	0.875	0.890	0.005
p014	0.893	0.600	0.912	0.560	0.019
p015	0.995	0.790	0.995	0.810	0.000
avg	0.881	0.825	0.893	0.836	0.012
std	0.037	0.083	0.035	0.101	0.006
min	0.838	0.600	0.855	0.560	0.000
max	0.995	0.910	0.995	0.930	0.019

described since the data could not practically be acquired as quickly as necessary to ignore such a model or correction term.

When including the TOF information, the impact of neglecting the coil attenuation is reduced, but only by a small fraction of the overall impact. This result is consistent with current PET/CT TOF resolution for this system, which is on the order of 550 ps [19] and has the main impact of reducing noise for larger patients. This improvement with TOF can also be seen in the percent difference comparison shown in Fig. 7.

Inspection of the joint histogram results in Table 2, which account for changes throughout the full PET image volume, shows that both reconstruction methods perform well in maintaining the full-volume PET quantitation. Including TOF information moves the slope of the fit line slightly toward the identity line, but only by a small amount. This type of image data analysis has utility in that the performance over the whole image can be condensed into a single metric, in order to compare two approaches and determine which produces a result closer to the baseline approach.

Visual inspection of the PET images and image differences across all subjects demonstrated that the image changes were mostly distributed throughout the image volume and were not apparent due to focal artifacts. This is important since one of the primary imaging goals is lesion detection, and loss of detection capability due to streaks or other inaccurate correction artifacts prioritizes the need to change coil design or incorporate methods to correct for the coil attenuation in a combined PET/MR system. Given that this coil is both flexible and designed to be placed according to patient anatomy over a wide range of patient sizes, approaches for coil localization are complex and likely prone to localization errors [9, 11] which may be on the order of the error induced by simply neglecting the coil attenuation. The comparison results that appear to be outliers, evident in Fig. 7 for P007, P009, P010 and P015, are potentially due to either liver FDG clearance that does not follow that demonstrated in Laffon et al., i.e. reconstruction noise near the edges of the field of view, or patient motion. Inspection of the images for these cases as part of the clinical evaluation did not implicate any cause related to presence of the AA coil, and both the coil-present and coil-absent PET image data were similar to other cases.

For the clinical comparison, there is currently no data available in the literature comparing the diagnostic impact of having a coil within the FOV of the PET as compared to the coil-absent images (with the exception of a single patient measurement reported in [11], where the coil caused a bias of −11.4 % on a pancreas carcinoma). Early PET/MRI evaluations did not report any significant image artifacts noted from the coil [20–22]. However, these studies did not compare with non-coil images. Additionally, the physiologic decay was not taken into account in any of the available studies. Thus, the results presented here represent to our opinion the most relevant evaluation of the diagnostic impact of a coil within the FOV when its attenuation is not accounted for.

Similar phenomena concerning the diagnostic relevance have been recently reported when comparing CT-AC and MR-AC imaging [23]. For consistency in the lesion to background ratio, our study included only FDG whereas tracers beyond FDG were included in the evaluation in [23]. Even though significant differences were found in the quantitation of liver uptake, no significant clinical impact was demonstrated. Further efforts are currently being undertaken to determine and correct coil attenuation that include more sophisticated sequences that can also be used for MR-AC, such as ultra-short TE [24]. The results presented here represent a lower limit on the accuracy required when accounting for the coil attenuation.

The results presented in this study are limited to the GE GEM anterior array coil, but are likely to be similar for other flat, flexible coils of similar size and composition. New coil designs with lighter casing materials and optimized arrangement of the more massive electronic components may further reduce the errors introduced by the coil. The procedures described here can be easily applied to evaluate other coils and coil configurations (e.g. the

peripheral-vascular array). One factor that will need further study is the impact of the coil cable attenuation, in those cases where the cable cannot be placed away from the structures of interest.

A considerable limitation of our study is certainly the small number of patients. However, it represents a first study to compare coil-present to coil-absent imaging in patients using a standard clinical coil and it demonstrates results in both a technical and in a clinical diagnostic way. Further, the results account for tracer redistribution, which is necessary in dual-time-point studies when looking for small SUV differences not caused by physiologic change over time.

Conclusion

The results demonstrate that use of the MR anterior array coil did produce statistically significant but generally small changes in liver SUV, approximately on the order of 5 %. No clinically significant differences were demonstrated when the coil was used within the PET-FOV. Further, only a slight decrease in lesion conspicuity during the clinical analysis of pathologic lesions was noted in the images with the coil present for three of 15 patients, which could potentially be due to increased image noise from the later imaging time for the coil-present images. Further efforts are underway to validate the robustness of these comparative analysis methods on a larger patient population, as well as to identify coil design improvements that will lead to increased PET quantification accuracy.

Acknowledgments The authors would like to thank Prof. G. K. von Schulthess and collaborators at the University Hospital of Zurich for collection of and access to the patient data used in this study.

References

1. Martinez-Moller A, Souvatzoglou M, Delso G, Bundschuh RA, Chefd'hotel C, Ziegler SI, Navab N, Schwaiger M, Nekolla SG (2009) Tissue classification as a potential approach for attenuation correction in whole-body PET/MRI: evaluation with PET/CT data. J Nucl Med 50(4):520–526
2. Hofmann M, Pichler B, Scholkopf B, Beyer T (2009) Towards quantitative PET/MRI: a review of MR-based attenuation correction techniques. Eur J Nucl Med Mol Imaging 36(Suppl 1): S93–104
3. Keereman V, Holen RV, Mollet P, Vandenberghe S (2011) The effect of errors in segmented attenuation maps on PET quantification. Med Phys 38(11):6010–6019
4. Keereman V, Mollet P, Berker Y, Schulz V, Vandenberghe S (2012) Challenges and current methods for attenuation correction in PET/MR. Magn Reson Mater Phy 26(1):81–98
5. Schramm G, Langner J, Hofheinz F, Petr J, Beuthien-Baumann B, Platzek I, Steinbach J, Kotzerke J, van den Hoff J (2012) Quantitative accuracy of attenuation correction in the Philips Ingenuity TF whole-body PET/MR system: a direct comparison with transmission-based attenuation correction. Magn Reson Mater Phy 26(1):115–126
6. Keller SH, Holm S, Hansen AE, Sattler B, Andersen F, Klausen TL, Hojgaard L, Kjaer A, Beyer T (2013) Image artifacts from MR-based attenuation correction in clinical, whole-body PET/MRI. Magn Reson Mater Phy 26(1):173–181
7. MacDonald LR, Kohlmyer S, Liu C, Lewellen TK, Kinahan PE (2011) Effects of MR surface coils on PET quantification. Med Phys 38(6):2948–2956
8. Bin Z, Pal D, Zhiqiang H, Ojha N, Guo T, Muswick G, Chi-hua T, Kaste J (2009) Attenuation correction for MR table and coils for a sequential PET/MR system. In: Proceedings of IEEE Nuclear Science Symposium (NSS/MIC), pp 3303–3306
9. Tellmann L, Quick HH, Bockisch A, Herzog H, Beyer T (2011) The effect of MR surface coils on PET quantification in whole-body PET/MR: results from a pseudo-PET/MR phantom study. Med Phys 38(5):2795–2805
10. Delso G, Martinez-Moller A, Bundschuh RA, Ladebeck R, Candidus Y, Faul D, Ziegler SI (2010) Evaluation of the attenuation properties of MR equipment for its use in a whole-body PET/MR scanner. Phys Med Biol 55(15):4361–4374
11. Paulus DH, Braun H, Aklan B, Quick HH (2012) Simultaneous PET/MR imaging: MR-based attenuation correction of local radiofrequency surface coils. Med Phys 39(7):4306–4315
12. Thie JA, Hubner KF, Smith GT (2002) Optimizing imaging time for improved performance in oncology PET studies. Mol Imaging Biol 4(3):238–244
13. Boellaard R, O'Doherty MJ, Weber WA, Mottaghy FM, Lonsdale MN, Stroobants SG, Oyen WJ, Kotzerke J, Hoekstra OS, Pruim J, Marsden PK, Tatsch K, Hoekstra CJ, Visser EP, Arends B, Verzijlbergen FJ, Zijlstra JM, Comans EF, Lammertsma AA, Paans AM, Willemsen AT, Beyer T, Bockisch A, Schaefer-Prokop C, Delbeke D, Baum RP, Chiti A, Krause BJ (2010) FDG PET and PET/CT: EANM procedure guidelines for tumour PET imaging: version 1.0. Eur J Nucl Med Mol Imaging 37(1): 181–200
14. Binns DS, Pirzkall A, Yu W, Callahan J, Mileshkin L, Conti P, Scott AM, Macfarlane D, Fine BM, Hicks RJ (2011) Compliance with PET acquisition protocols for therapeutic monitoring of erlotinib therapy in an international trial for patients with non-small cell lung cancer. Eur J Nucl Med Mol Imaging 38(4): 642–650
15. Choi WH, Yoo IR, O JH, Kim SH, Chung SK (2011) The value of dual-time-point 18F-FDG PET/CT for identifying axillary lymph node metastasis in breast cancer patients. Br J Radiol 84(1003):593–599
16. Zytoon AA, Murakami K, El-Kholy MR, El-Shorbagy E (2008) Dual time point FDG-PET/CT imaging… Potential tool for diagnosis of breast cancer. Clin Radiol 63(11):1213–1227
17. Conti M (2011) Why is TOF PET reconstruction a more robust method in the presence of inconsistent data? Phys Med Biol 56(1):155–168
18. Laffon E, Adhoute X, de Clermont H, Marthan R (2011) Is liver SUV stable over time in (1)(8)F-FDG PET imaging? J Nucl Med Technol 39(4):258–263
19. Bettinardi V, Presotto L, Rapisarda E, Picchio M, Gianolli L, Gilardi MC (2011) Physical performance of the new hybrid PETCT Discovery-690. Med Phys 38(10):5394–5411
20. Drzezga A, Souvatzoglou M, Eiber M, Beer AJ, Furst S, Martinez-Moller A, Nekolla SG, Ziegler S, Ganter C, Rummeny EJ, Schwaiger M (2012) First clinical experience with integrated whole-body PET/MR: comparison to PET/CT in patients with oncologic diagnoses. J Nucl Med 53(6):845–855
21. Schwenzer NF, Schraml C, Muller M, Brendle C, Sauter A, Spengler W, Pfannenberg AC, Claussen CD, Schmidt H (2012)

Pulmonary lesion assessment: comparison of whole-body hybrid MR/PET and PET/CT imaging–pilot study. Radiology 264(2): 551–558

22. Eiber M, Martinez-Moller A, Souvatzoglou M, Holzapfel K, Pickhard A, Loffelbein D, Santi I, Rummeny EJ, Ziegler S, Schwaiger M, Nekolla SG, Beer AJ (2011) Value of a Dixon-based MR/PET attenuation correction sequence for the localization and evaluation of PET-positive lesions. Eur J Nucl Med Mol Imaging 38(9):1691–1701
23. Wiesmuller M, Quick HH, Navalpakkam B, Lell MM, Uder M, Ritt P, Schmidt D, Beck M, Kuwert T, von Gall CC (2013) Comparison of lesion detection and quantitation of tracer uptake between PET from a simultaneously acquiring whole-body PET/MR hybrid scanner and PET from PET/CT. Eur J Nucl Med Mol Imaging 40(1):12–21
24. Catana C, Van der Kouwe A, Benner T, Hamm C, Michel CJ, Fenchel M, Byars L, Schmand M, Sorensen AG (2010) MR-Based PET attenuation correction for neurological studies using dual-echo UTE sequences. Proceedings of Joint Annual Meeting of the International Society of Magnetic Resonance in Medicine and the European Society for Magnetic Resonance in Medicine and Biology, Stockholm, p 3953